Time-Resolved Fluorescence Resonance Energy Transfer Shows that the Bacterial Multidrug ABC Half-Transporter BmrA Functions as a Homodimer †

ARTICLE *in* BIOCHEMISTRY · APRIL 2005

Impact Factor: 3.02 · DOI: 10.1021/bi0482809 · Source: PubMed

Time-Resolved Fluorescence Resonance Energy Transfer Shows that the Bacterial Multidrug ABC Half-Transporter BmrA Functions as a Homodimer†

Olivier Dalmas,‡ Marie-Ange Do Cao,‡ Miguel R. Lugo,§ Frances J. Sharom,§ Attilio Di Pietro,‡ and Jean-Michel Jault*,‖

Institut de Biologie et Chimie des Protéines, UMR 5086 CNRS-UCBL1 and IFR 128, 7 passage du Vercors, 69367 Lyon Cedex 07, France, Department of Molecular and Cellular Biology, University of Guelph, Guelph, Ontario, Canada N1G 2W1, and Laboratoire de Biophysique Moléculaire et Cellulaire, DRDC, UMR 5090 CNRS/CEA/UJF, CEA 17 rue des Martyrs, Bâtiment K, 38054 Grenoble Cedex 9, France

Received August 10, 2004; Revised Manuscript Received January 17, 2005

ABSTRACT: Members of the ATP-binding cassette (ABC) transporters share the same basic architecture, with a four-core domain made of two transmembrane plus two nucleotide-binding domains. However, a supramolecular organization has been detected in some ABC transporters, which might be relevant to physiological regulation of substrate transport. Here, the oligomerization status of a bacterial half-ABC multidrug transporter, BmrA, was investigated. Each BmrA monomer containing a single cysteine residue introduced close to either the Walker A or the ABC signature motifs was labeled using two probes, 2-(4-maleimidoanilino)naphthalene-6-sulfonic acid (fluorescence donor) or 4-dimethylaminophenylazophenyl-4′-maleimide (fluorescence acceptor). Reconstitution into proteoliposomes of BmrA monomers labeled separately with either the fluorescence donor or the fluorescence acceptor allowed measurement of time-resolved fluorescence resonance energy transfer between the two probes, showing that efficient reassociation of the singly labeled BmrA monomers occurred upon reconstitution. The efficiency of energy transfer studied as a function of increasing concentration of BmrA-labeled with the fluorescence acceptor argues for a dimeric association of BmrA instead of a tetrameric one. Furthermore, the efficiency of energy transfer allowed estimation of the distances between the two bound probes. Results suggest that, in the resting state, BmrA in a lipid bilayer environment preferentially adopts a closed conformation similar to that found in the BtuCD crystal structure and that the presence of different effectors does not substantially modify its global conformation.

ATP-binding cassette (ABC)[1] transporters are widely distributed among all living organisms. They are involved in the unidirectional transport, either import or export, of many different substrates, including ions, sugars, lipids, amino acids, proteins, and xenobiotics (*1*). In bacteria, they often represent the largest protein family with, for instance, almost 5% of the *Escherichia coli* genome (*2*) and 78 members in *Bacillus subtilis* (*3*). In humans, 48 ABC transporters have been identified, and the abnormal functioning of some of them is often associated with severe pathologies (*4*). Hence, *P*-glycoprotein, the first mammalian ABC transporter identified, was shown to be involved in multidrug resistance in cancer cells (*5*). Also, mutations in the chloride channel CFTR were identified as the genetic basis for cystic fibrosis (*6*).

The overall architecture is conserved among all ABC transporters, which are made up of four core structural units, including two transmembrane domains and two nucleotide-binding domains (NBDs). The former, which is quite variable in sequence and topology, defines the substrate-binding site, while the latter, which is more conserved in sequence, powers the transporter by binding and hydrolyzing ATP (*1*, *7*). These four domains are either fused as a single polypeptide in most eukaryotic ABC transporters (full-length transporters) or found on separate polypeptides, from two (half-transporters) to four subunits. Three-dimensional structures have been obtained for many isolated NBDs from various origins, and they all shared the same global topology (*8*, *9*). The physical interactions triggering the NBDs dimerization have been quite controversial for a long time, but it is now believed that a transient association between the two ATP-binding sites shared between the NBDs reflects one of the functional conformations that ABC transporters can adopt (*10*, *11*). On the other hand, the high-resolution structures of three full-length ABC transporters have been determined: two structures involved the lipid A exporter MsbA (from *E. coli* and

† This work was supported by a grant from the CNRS ATIP "Young Investigator" Program to J.-M.J., CNRS Grants PCV 2001 and PGP 2002 to A.D.P., an ACI IMPBio Grant (IMPB027) from the "Ministère de la Recherche" to A.D.P. and J.-M.J., and a grant from the National Cancer Institute of Canada (with funds provided by the Canadian Cancer Society) to F.J.S.; O.D. and M.-A.D.C. are recipients of a fellowship from the "Ministère de l'Enseignement Supérieur". O.D. is also a recipient of a fellowship from the "Région Rhônes-Alpes, EURODOC Program" and from the "Centre Jacques Cartier".

* To whom correspondence should be addressed. Fax: 33-4-38-78-54-87. Telephone: 33-4-38-78-31-19. E-mail: jean-michel.jault@cea.fr.

‡ Institut de Biologie et Chimie des Protéines.

§ University of Guelph.

‖ Laboratoire de Biophysique Moléculaire et Cellulaire.

[1] Abbreviations: ABC, ATP-binding cassette; DABMI, 4-dimethylaminophenylazophenyl-4′-maleimide; DDM, *n*-dodecyl-*β*-D-maltoside; FRET, fluorescence resonance energy transfer; MIANS, 2-(4-maleimidoanilino)naphthalene-6-sulfonic acid; NBD, nucleotide-binding domain; Vi, orthovanadate.

10.1021/bi0482809 CCC: $30.25
Published on Web 00/00/0000 PAGE EST: 10

Vibrio cholerae), and the third one was obtained for the vitamin B_{12} importer, BtuCD (*12*−*14*). These three structures exhibited quite divergent features, with *E. coli* MsbA existing in an open conformation, characterized by the two NBDs being separated by ∼20 Å (*12*), while both *V. cholerae* MsbA and BtuCD were crystallized in a closed conformation. However, whereas the two ATP-binding sites of BtuCD were located at the interface of the NBDs (*13*), the NBDs from *V. cholerae* MsbA adopted an unprecedented conformation, with the two ATP-binding sites being only partly located at their interface (*14*).

Oligomeric assembly has been reported for several ABC transporters including full-length transporters such as *P*-glycoprotein (*15*−*17*), the multidrug resistance protein (*18*, *19*), the Pdr5p yeast multidrug transporter (*20*), and very recently the half-transporter BCRP (or ABCG2) (*21*). These findings raised the possibility that a di- or tetrameric organization might be the functional unit for full-length or half-ABC transporters, respectively. Recently, we have characterized a new bacterial multidrug half-ABC transporter, named BmrA (for *Bacillus* multidrug-resistance ATP) (*22*) and formerly known as YvcC (*23*), whose 3D structure, previously solved at low resolution by cryoelectron microscopy, suggested an organization of at least a homodimer and possibly a homotetramer (*24*). Here, the supramolecular organization of BmrA was investigated by using fluorescence resonance energy transfer (FRET), because this technique allows efficient discrimination between different oligomers of the functional unit for a protein (*25*). To circumvent some uncertainties inherent to this technique and in particular the need for accurate quantification of the concentration of the fluorescent donor in the presence of the fluorescent acceptor, a time-resolved approach was used to monitor more accurately the energy-transfer efficiency (*26*). The results obtained strongly suggest that, in a lipid bilayers environment, BmrA forms a homodimer and not a homotetramer. In addition, the energy-transfer efficiency measured between the two fluorescent probes, with each probe being tethered to one BmrA monomer, suggests that BmrA adopts mainly a conformation relevant to that found in the BtuCD transporter, with the two ATP-binding sites located at the interface of the NBDs.

EXPERIMENTAL PROCEDURES

Unless stated otherwise, products were purchased from Sigma.

Site-Directed Mutagenesis. pET23b(+)/*yvcC* constructed as previously described (*23*) was used as a template for site-directed mutagenesis. First, the cysteine-less mutant C436S was designed using Kunkel's method as previously described (*27*), with 5′-TCTAACCCGTAGGAAATGTTTTCTCT-GATTGT-3′ as a primer to introduce a single amino acid mutation and a conservative mutation deleting one *Ssp*I restriction site to allow the screening of positive clones. pET23b(+)/*C436S* was therefore used as a template for single-cysteine introduction. T370C mutant and S428C were designed using 5′-CGGACCGACGATCGCACACACTTT-GCCGGCTTCAATGACGGC-3′ and 5′-ATATTTTCTCT-GATGGTACCGCACATTAACGGGC-3′ as primers, respectively, and introducing either a *Kpn*I or *Nae*I restriction site to screen for positive clones, respectively. The G473C mutation was performed using a QuikChange Site-Directed Mutagenesis Kit (Stratagene). Oligonucleotides were designed as follows: to introduce the single amino acid mutation, 5′-GCCGAATCAGTTTGATACAGAAGTGTC-GAACGCGGCATTATGCTGTC-3′ was used as the upstream primer and 5′-GACAGCATAATGCCGCGTTCG-CACACTTCTGTATCAAACTGATTCGGC-3′ was used as the downstream primer. Positive clones were selected by overall gene sequencing.

BmrA Purification. Bacteria were grown at 30 °C, and a 4 h induction with 0.7 mM IPTG was performed when OD_{600nm} reached 1−2. All of the subsequent steps were done as previously described (*23*, *27*). This method allowed us to prepare 3 mg of pure BmrA per liter of culture.

Protein Labeling. Frozen protein aliquots were rapidly thawed, and β-mercaptoethanol was removed using a BioRad Econo-Pac 10DG desalting column (exclusion limit 6000 Da) previously equilibrated with the labeling buffer [50 mM Hepes at pH 7, 50 mM NaCl, 5 mM $MgCl_2$, and 0.05% (w/v) DDM]. Then, a 5-fold molar excess of either MIANS (Molecular Probes Inc., Eugene, OR) or DABMI (Molecular Probes) was added under stirring to a 1 mg mL^{-1} protein solution at room temperature, in the absence of light. After 1 h, the reaction was stopped by the addition of 1 mM DTE, and the excess of the quenched probes was removed by a desalting column previously equilibrated with 50 mM Hepes at pH 8, 50 mM NaCl, 5 mM $MgCl_2$, and 0.05% (w/v) DDM.

The stoichiometry of labeling was calculated by spectrophotometry using the following parameter for the DABMI derivative, $\epsilon_{280} = 9980\ M^{-1}\ cm^{-1}$. The extinction coefficients were determined from titration curves following the reaction of the fluorescent probe with *N*-acetylcysteine in the same sample buffer. All absorption spectra were recorded on a Varian Cary 50 UV−visible spectrophotometer. The protein extinction coefficient, $\epsilon_{280} = 39\,800\ M^{-1}\ cm^{-1}$, was calculated on the NPSA server (http://npsa-pbil.ibcp.fr) from the primary sequence of BmrA.

The protein concentration was calculated using the equation

$$[\mathrm{BmrA}] = \frac{\mathrm{OD}_{280} - \mathrm{OD}_{\lambda_{max}} \dfrac{\epsilon_{280}^{probe}}{\epsilon_{\lambda_{max}}^{probe}}}{\epsilon_{280}^{protein} l} \quad (1)$$

The stoichiometry of probe to protein was calculated, and the reaction times were optimized to achieve a ratio ≤1.

Proteoliposome Reconstitution. Briefly, 2−4 mg of *E. coli* total phospholipid extract (Avanti Polar lipids Alabaster, AL) was dried under a stream of nitrogen and then pumped in a vacuum for 1 h. Reconstitution buffer [50 mM Hepes at pH 8, 50 mM NaCl, and 5 mM $MgCl_2$ (or 5 mM $CoCl_2$ where indicated)] was added to give a 25 mg mL^{-1} lipid concentration, and the suspension was incubated under stirring at room temperature with 20 μL of 10% DDM (Alexis Biochemicals). After 1 h, 100−200 μg of unlabeled protein or protein labeled with either MIANS or DABMI was added in a final volume of 600−1200 μL of reconstitution buffer. After incubation for 45 min, 3 successive additions of 40−80 mg of Bio-Beads SM2 (Bio-Rad Laboratories) were performed every hour. Then, the proteoliposomes were centrifuged at 200000*g*

for 35 min, suspended in a final volume of 700 μL of reconstitution buffer, and kept on ice until use.

ATPase Assay. The ATPase activity was measured using the P_i release method (*28*). Briefly, proteoliposomes were added to the reaction mixture containing 50 mM Hepes/NaOH at pH 8, 50 mM NaCl, 5 mM $CoCl_2$, 5 mM ATP, 9 mM PEP, and 20 units mL^{-1} pyruvate kinase.

Vanadate Trapping. A total of 0.5 mM freshly boiled orthovanadate solution was added to proteoliposomes suspended in reconstitution buffer containing 5 mM $CoCl_2$ and supplemented with 0.01% DDM. After 20 min of incubation at 30 °C, 5 mM ATP was added and the mixture was further incubated at the same temperature for 20 min. $CoCl_2$ was preferred instead of $MgCl_2$ for the vanadate trapping experiment, because it was found to produce an inhibited-trapped state of BmrA more stable ($t_{1/2}$ for the reactivation >10 h) than the $MgCl_2$ one, in agreement with the results found with the *P*-glycoprotein (*29*).

Proteoliposomes Permeabilization. Proteoliposome integrity was checked with an assay based on calcein [(2′,7′-[bis-(carboxymethyl)amino]methyl)fluorescein] fluorescence (*30*). Basically, proteoliposomes were prepared in reconstitution buffer supplemented with 0.8 mM calcein and 5 mM cobalt. The time course of fluorescence intensity (λ_{ex} = 490 nm and λ_{em} = 520 nm) was followed on an Alphascan-2 spectrofluorimeter (Photon Technology International, London, Ontario, Canada), with the cell holder thermostated at 25 °C. The slits were set at 2 and 4 nm for excitation and emission, respectively. A total of 10 mM EDTA was then added, and an increase in fluorescence intensity was directly related to the permeability of the proteoliposomes. To determine the lowest concentration of DDM required to render the proteoliposomes leaky, they were preincubated at 30 °C for 30 min with an increasing concentration of DDM and the fluorescence intensity was then monitored after addition of 10 mM EDTA. A total of 0.2% (v/v) Triton X-100 was then added inside the cuvette to completely solubilize the proteoliposomes and thus obtain the maximal level of fluorescence intensity. An increase in fluorescence after addition of Triton X-100 showed that the DDM concentration used in the pretreatment was too low to fully permeabilize the proteoliposomes. It was found that 0.01% DDM was the lowest concentration capable to totally permeabilize the proteoliposome mixture.

Steady-State Measurements and Determination of the Parameters for FRET Analysis. Fluorescence spectra were recorded on an Alphascan-2 spectrofluorimeter (Photon Technology International, London, Ontario, Canada), with the cell holder thermostated at 25 °C. The excitation and emission slits were both set at 4 nm. The quantum yield of BmrA-MIANS, Q_D, was determined for each mutant at an excitation wavelength of 322 nm, relative to a standard solution of quinine sulfate in 0.1 N H_2SO_4, using polarizers oriented at the magic angle (excitation polarizer set vertical, and emission polarizer set at 54.7°). The quantum yield of labeled MIANS-BmrA was calculated using the equation

$$Q_{\mathrm{MIANS-BmrA}} = \left(\frac{F_{\mathrm{MIANS-BmrA}}}{F_{\mathrm{quinine}}}\right)\left(\frac{A_{\mathrm{quinine}}}{A_{\mathrm{MIANS-BmrA}}}\right)Q_{\mathrm{quinine}} \quad (2)$$

where Q_{quinine}, the quantum yield of quinine, is known to be 0.546 in 0.1 N H_2SO_4, $F_{\mathrm{MIANS-BmrA}}$ and F_{quinine} are the integrals of fluorescence in the wavelength range of 350−600 nm, and $A_{\mathrm{MIANS-BmrA}}$ and A_{quinine} are the absorbance values at 322 nm. The quantum yield of MIANS-BmrA was calculated in the presence or absence of the substrate.

The efficiency of energy transfer, *E*, defined as

$$E = 1 - \frac{\tau_{\mathrm{DA}}}{\tau_{\mathrm{D}}} \quad (3)$$

where τ_{DA} and τ_D are the lifetime of the donor in the presence and absence of the acceptor, respectively. *E* is related to the inverse 6th power of the distance, *R*, between the donor and the acceptor according to the equation

$$R = R_0\left(\frac{1}{E} - 1\right)^{1/6} \quad (4)$$

R_0 is the distance at which the transfer efficiency is 50% and is calculated as followed

$$R_0 = 0.211(J\kappa^2 Q_{\mathrm{D}} n^{-4})^{1/6} \quad (5)$$

The orientation factor κ^2 was taken as $^2/_3$, which represents the case where the donor and acceptor both rotate rapidly relative to the donor lifetime; the refractive index of the medium, *n*, generally between 1.3 and 1.4, was taken as 1.33; *J* (in M^{-1} cm^{-1} nm^4) is the spectral overlap integral between the emission spectrum of the donor, F_D, and the absorbance spectrum of the acceptor, ϵ_A, as follows

$$J = \frac{\int F_{\mathrm{D}}(\lambda)\epsilon_{\mathrm{A}}(\lambda)\lambda^4\delta\lambda}{\int F_{\mathrm{D}}(\lambda)\delta\lambda} \quad (6)$$

Time-Resolved Measurements. The experiments were carried out on a TimeMaster Model TM-4 **(**Photon Technology International, London, Ontario, Canada) supplied with a nitrogen/dye LASER, using the pulse-sampling method (*31*). For the measurements, the dye laser output at 644 nm was frequency-doubled to 322 nm and the excitation was recorded via a polarizer set at 35.3°, a cut-on glass filter at 380 nm (to reject the scattered light), and a monochromator set at 420 nm (22 nm slit) by a stroboscopic-controlled photomultiplier. The proteoliposome suspension was kept on ice, and the buffer was ice-chilled before lifetime measurements were carried out at 2 °C. The fluorescence intensity was recorded during 80 ns, within 400 channels (1 channel = 0.2 ns), and for each decay, 35 readings per channel were performed (7 averages and 5 shots). The instrumental response function (IRF) was recorded under the same conditions at the excitation wavelength by replacing the sample with a scattering solution of colloidal silica (LUDOX, Grace). The fluorescence intensity decay was analyzed using FELIX32 software. The observed decay of the sample, $R(t)$, is the convolution of the δ-pulse response of the sample, $I(t)$, with the instrument response function, $E(t)$, by

$$R(t) = E(t) \otimes I(t) = \int_{-\infty}^{t} E(t')I(t - t')\,\mathrm{d}t' \quad (7)$$

The software uses an iterative-fitting procedure based on the Marquardt algorithm to minimize the deviation of the experimental data, $R(t)$, with the result of the convolution of the registered IRF with a decay model, $I(t)$, presented as

the sum of the 1−4-exponential decay function by

$$I(t) = \sum_i \alpha_i e^{(-t/\tau_i)} \quad (8)$$

where α_i values are the pre-exponential factor or amplitude and τ_i values are the average lifetime of each component of the decay. Deviations from the best fit are characterized by the reduced chi-squared (χ_r^2) statistic. The time-course values of the fluorescence intensity were fitted to a sum of exponentials. The number of exponentials was iteratively increased until the χ_r^2 did not improve. When necessary, light-scattering contribution was eliminated by fixing a very short lifetime component such as 1 ps, and the remaining two lifetimes were used to calculate the amplitude-average lifetime. In addition to the value of χ_r^2, graphical tests such as the plot of weighted residuals were used to assess the accuracy of the fit. Then, for each fluorescence intensity decay, the amplitude-average lifetime was calculated as follows:

$$\langle\tau\rangle_a = \frac{\sum_{i=1}^{n} \alpha_i \tau_i}{\sum_{i=1}^{n} \alpha_i} = \sum_{i=1}^{n} a_i \tau_i \quad (9)$$

Statistical Analysis of the FRET Phenomenon. An important parameter is the probability of formation of a hybrid transporter, i.e., the probability of having one monomer labeled with the donor fluorophore associated with at least one monomer labeled with the acceptor fluorophore. If we consider the dimer model, six different species of dimer might be present within the lipid bilayer. In the following expressions, *a* and *d* are the molar fractions of the acceptor and the donor respectively, 0 means the lack of chromophore (i.e., without labeling), D refers to BmrA labeled with MIANS (the donor), and A refers to BmrA labeled with DABMI (the acceptor). Assuming that the association between two monomers is noncooperative, random, and of equal strength for all labeled species, we thus have different probabilities of association: $P(D,D) = d^2$; $P(D,0) = 2d(1 - d - a)$; $P(D,A) = 2ad$; $P(A,A) = a^2$; $P(A,0) = 2a(1 - a - d)$; and $P(0,0) = (1 - a - d)^2$.

Because only the MIANS fluorescence is measured (DABMI being a nonfluorescent probe), only $P(D,D)$, $P(D,0)$, and $P(D,A)$ come into play in the observed phenomenon. Because energy transfer leads to a shorter amplitude-average lifetime $\bar{\tau}$, we could express the average of the different fluorescence component weighted by their probability of association as follows:

$$\bar{\tau} = \frac{[2P(D,D) + P(D,0)]\bar{\tau}_D + P(D,A)\bar{\tau}_{DA}}{[2P(D,D) + P(D,0) + P(D,A)]} = \bar{\tau} = (\bar{\tau}_{DA} - \bar{\tau}_D)a + \bar{\tau}_D \quad (10)$$

and $\bar{\tau}_{DA}$ can be determined from the slope of the plot between the amplitude-average lifetime and the molar fraction of the acceptor. All linear regressions were performed with SigmaPlot 8.0 (SPSS Inc).

Determination of the Oligomerization State of BmrA. The efficiency of energy transfer according to different models of BmrA oligomerization was performed as described previously (*25*). Theoretical curves were constructed using the equation $\tau_{DA}/\tau_D = 1 - E + E(1 - a)^{n-1}$, where *n* is the degree of oligomerization (for instance, $n = 2$ for a dimer).

RESULTS

To monitor FRET between two bound probes, one on each BmrA monomer, the unique cysteine residue present on BmrA (C436) was first removed by site-directed mutagenesis to construct a cysteine-less mutant (C436S). This mutation did not alter the transport properties of BmrA (not shown). Next, a single-cysteine residue was introduced into the BmrA sequence as indicated in Figure 1. We introduced these new cysteines, separately, close to either the Walker A (T370C) or the ABC signature motifs (G473C) because these two conserved sequences are believed to make up the ATP-binding site at the interface of the two NBDs, at least in a transient manner, during the catalytic cycle of ABC transporters (*10*, *11*, *13*). Caution was nevertheless taken to introduce these cysteine residues outside these two motifs to minimize perturbation of the structure of the NBD interface. Each single mutant studied separately transported the dye Hoechst 33342 (*22*) as efficiently as the wild-type enzyme, indicating that the newly introduced mutations did not affect the transport properties of BmrA (not shown).

BmrA mutants (T370C or G473C) were then labeled with either MIANS or DABMI probes, and the spectral properties of all of the labeled proteins were studied. The example in Figure 2A shows that the fluorescence emission spectrum of the BmrA T370C mutant labeled with MIANS overlaps fairly well with the absorbance spectrum of the same mutant labeled with DABMI, allowing for the calculation of the distance for 50% efficiency of energy transfer, R_0, of 31 Å. Similar calculations were made for the two other combinations of BmrA mutants: T370C labeled with MIANS plus G473C labeled with DABMI and G473C labeled with MIANS plus G473C labeled with DABMI. This yielded R_0 values of 30.9 and 31.4 Å, respectively (Table 1). Such R_0 values are well-suited to measure a transfer efficiency over a distance range of ∼15−45 Å between the two probes (*32*). Reconstitution of BmrA mutants covalently modified with MIANS into proteoliposomes containing a variable ratio of BmrA mutants derivatized with DABMI was then carried out. These experiments were performed at pH 8.0 because this is the optimal pH for either the ATPase activity of BmrA reconstituted in proteoliposomes and also for the drug transport activity measured with inverted-membrane vesicles (data not shown). Increasing the relative concentration of BmrA labeled with DABMI progressively increased the rate of fluorescence decay, indicating that energy transfer occurred between MIANS and DABMI (Figure 2B). The fitting of each curve was carried out using different exponential decays, and in all cases, the best fit was obtained with a three-exponential decay, as exemplified by the random distribution of the deviations between the experimental values and the fitted curve (see Figure 2C for one example). The values thus obtained for each molar ratio of acceptor probe and for the three different labeling combinations are reported in Table 2. The value of χ_r^2 calculated for each fit varied between 0.861 and 1.086, which reflects a reasonably correct

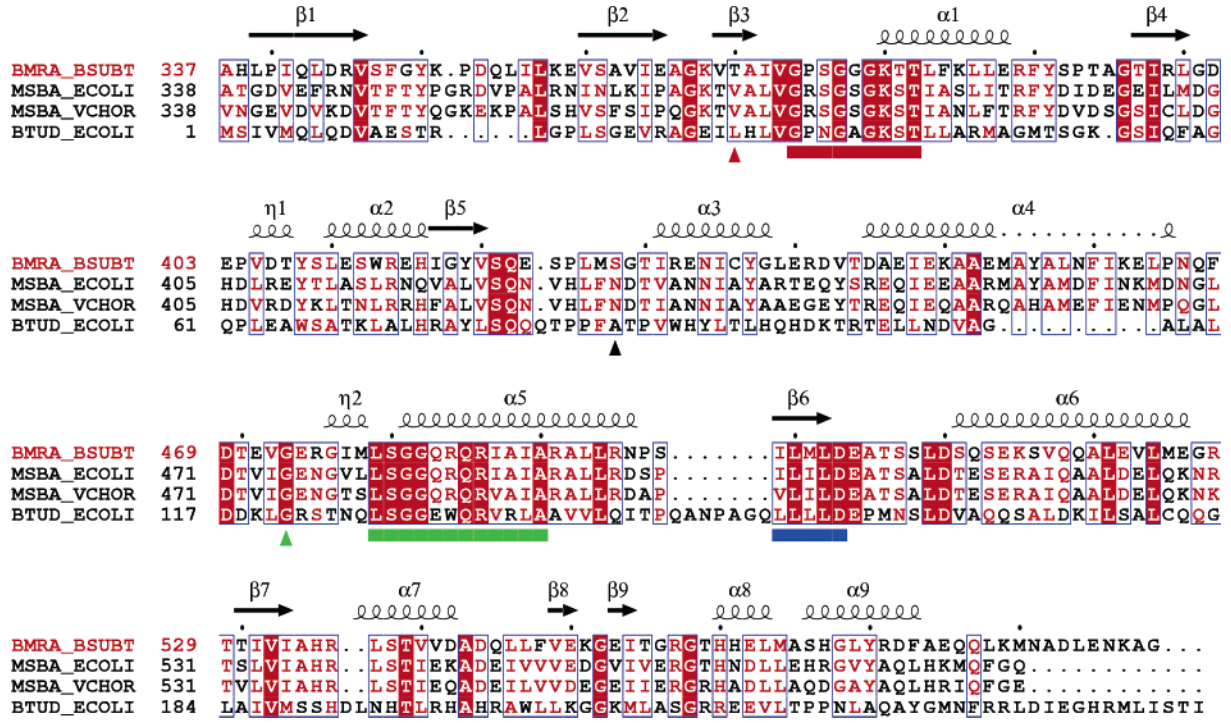

FIGURE 1: Sequence alignment of BmrA NBD with corresponding sequences of ABC transporters with known structures. Sequences were obtained on the ExPASy server (http://us.expasy.org/), and the alignment was generated by Clustal W (*45*) on the NPS@ server (http://www.ibcp.fr/). The BtuCD structure was downloaded from the Protein Data Bank (http://www.rcsb.org/pdb/) using 1L7V as the accession number. The abbreviations are BSUBT, *B. subtilis*; ECOLI, *E. coli*; and VCHOL, *V. cholerae*. The figure was made with ESPript 2.2 (http://prodes.toulouse.inra.fr/ESPript/). The secondary structures shown above the alignment were obtained from BtuD. Blue frames were drawn when at least 70% of the residues were conserved, with white characters in red boxes for strict identity and fully conserved residues and red characters for similarity. The position of the Walker A motif is underlined in red; the Walker B motif is underlined in blue; and the ABC signature motif is underlined in green. Positions of the newly introduced cysteine residues are shown by triangles using the same color code as the nearby conserved motifs; the S428C mutation is shown by ▲.

fitting (*33*). The amplitude average lifetime, $\langle\tau\rangle_a$, deduced from the curve fitting was then plotted as a function of the molar ratio of the probe acceptor (Figure 2D) for each combination of probe labeling, and the slopes of the straight lines obtained by linear regression analyses allowed us to deduce each τ_{DA} value (Table 3). These values were then used to calculate, using eq 3 given in the Experimental Procedures, the efficiency of energy transfer, *E*, whose values are reported in Table 3. The energy-transfer efficiencies were applied to theoretical models assuming that BmrA might exist either as a dimer, trimer, or tetramer in the membrane (*25*) and the theoretical curves obtained when the molar ratio of acceptor was plotted against the ratio of τ_{DA}/τ_D were compared with the experimental values. The results are shown in Figure 3A for the combination of the G473C mutant labeled with MIANS and the same mutant labeled with DABMI. Clearly, the best fit of the experimental values was obtained when the theoretical model was a homodimer, ruling out the possibility that BmrA functions as a homotetramer. Similar results were found when the two other probe combinations were used (parts B and C of Figure 3). It is important to note that the quality of the fit applied in Figure 2C did not really influence the outcome of the results shown in Figure 3 because applying a lower quality fit (for instance, one in which the amplitude of each component of the exponential decay was fixed but the lifetime was not) gave essentially the same results but with a higher scattering (not shown).

Finally, eq 4 was used to estimate the distances between the two bound probes, and the values reported in Table 3 favor a conformation where energy transfer between the two BmrA monomers occurs preferentially when the dimer adopts, in a resting state, a conformation similar to that found in the 3D structure of BtuCD but not in that of *E. coli* or *V. cholerae* MsbA.

Next, we wanted to analyze if the addition of nucleotides or drugs might affect either the oligomeric status of BmrA or the distance between the two monomers. However, the chemical derivatization of each mutant by either probe completely abolished the ATPase activity of BmrA, a property that might have been prejudicial to a correct interpretation of the results. Fortunately, we found that another mutant, the S428C located close to the so-called "Q-loop" (see Figure 1), kept ~20% ATPase activity after reconstitution with a 1:1 ratio of Cys-428−MIANS plus Cys-428−DABMI and a labeling stoichiometry of 1 mol/mol for each probe. Furthermore, this remaining ATPase activity was fully sensitive to inhibition by orthovanadate, a property shared by all ABC transporters including the wild-type BmrA (*22*). The time-resolved FRET experiments were then repeated with this new mutant, with a labeling combination of Cys-428−MIANS plus Cys-428−DABMI (Table 1), in the presence or absence of different effectors, namely, ATP/Co plus vanadate, ADP/Co, or doxorubicin, the latter being a substrate of BmrA (*22*). R_0 values between 30.9 and 28.4 Å were obtained in these experiments, depending on the effector used. Although the reconstitution protocol that we used seems to favor the "inside-out" orientation of BmrA in proteoliposomes, as testified by a very high ATPase activity after reconstitution (*22*), the presence of "right-side out"

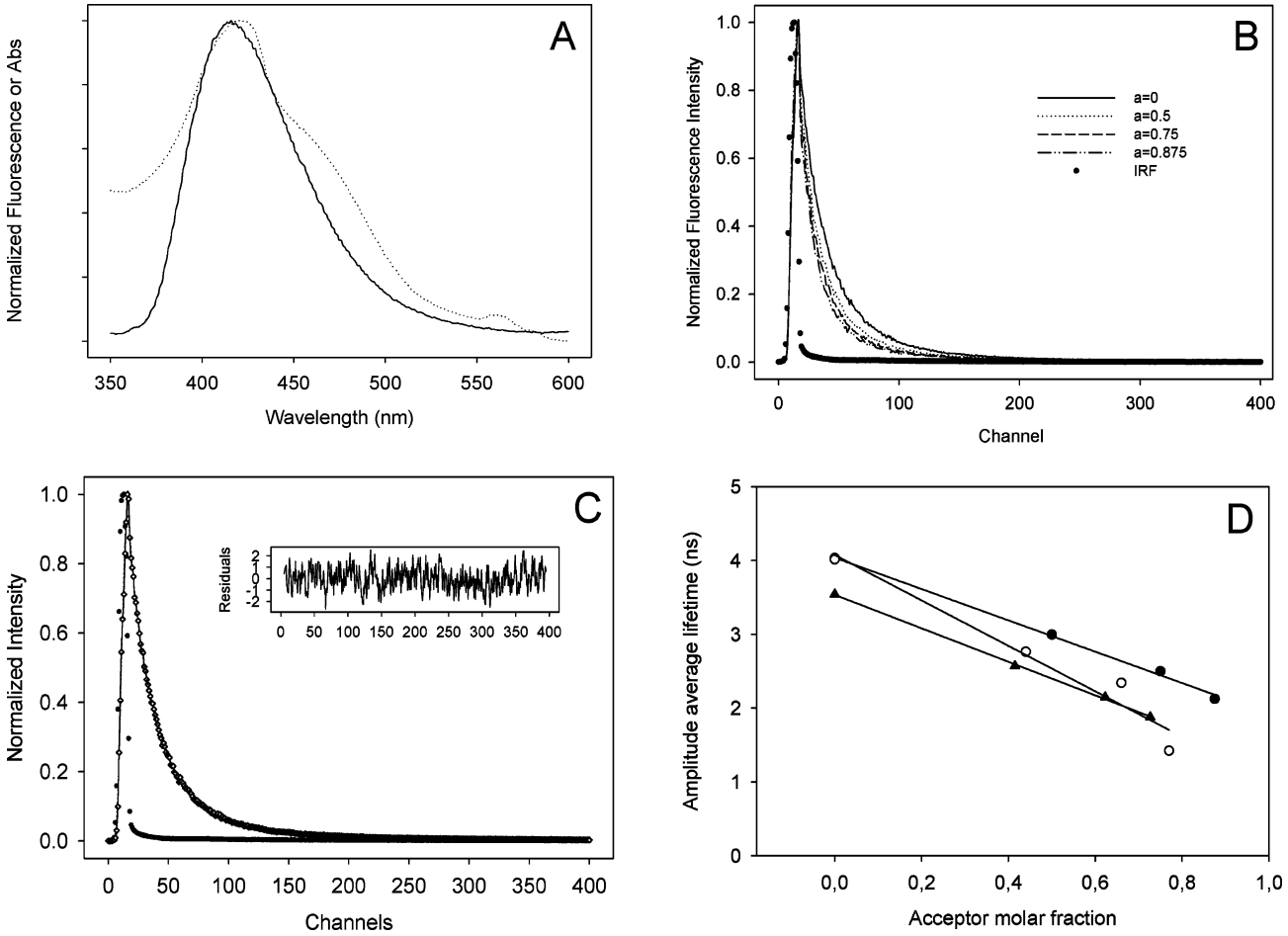

FIGURE 2: Resonance energy transfer in BmrA after reconstitution into liposomes. (A) Spectral overlap between the fluorescence emission spectrum of BmrA (T370C mutant) labeled with MIANS and the absorption spectrum of BmrA (T370C mutant) labeled with DABMI. The BmrA−MIANS fluorescence emission spectrum obtained by excitation at 322 nm is represented by a solid line, and the BmrA−DABMI absorption spectrum is shown as a broken line. The spectral overlap integral was calculated to determine the value of R_0 (see the Experimental Procedures). (B) Normalized fluorescence intensity of G473C−MIANS versus the channel number (1 channel = 0.2 ns) quenched by different molar fractions of G473C−DABMI; the instrument response function (IRF) is plotted as solid dots. (C) Three-exponential decay fitting of G473C−MIANS in the absence of G473C−DABMI; the IRF is plotted as solid dots; the experimental points are plotted as diamonds; and the three-exponential decay fitting is plotted as a thin line. The residual distribution function is shown in the inset. (D) Amplitude average lifetime versus the acceptor molar fraction for the reconstituted G473C−MIANS/G473C−DABMI, T370C−MIANS/T370C−DABMI, and G473C−MIANS/T370C−DABMI transporters are plotted with ●, ▲, and ○, respectively. The linear regression is plotted as a solid line for each combination.

BmrA in proteoliposomes could introduce a bias in these experiments, because these BmrA transporters would be unreachable to externally added effectors. Therefore, the proteoliposomes used in the presence of effectors were first incubated with the lowest concentration of DDM (0.01%) sufficient to make them leaky (see the Experimental Procedures). This pretreatment ensured that all BmrA molecules became equally accessible to the added effectors, while the ATPase activity was slightly increased (∼30%), showing that the conformation of the transporter was essentially unaltered by the presence of such a low concentration of DDM. The 30% increase in ATPase activity might actually reflect the proportion of "right-side out" BmrA molecules in the proteoliposomes mixture or, alternatively, could be due to a stimulatory effect of the detergent on the intrinsic ATPase activity of BmrA, because some detergents may be recognized as a substrate by multidrug ABC transporters such as *P*-glycoprotein (*34*). The results of the time-resolved FRET experiments performed on these proteoliposomes are reported in Table 2. In this set of experiments, a better fit was obtained with a two-exponential decay, rather than three, for both the control (Cys-428−MIANS and Cys-428−DABMI, without any effector) and the sample analyzed in the presence of ATP/Co and vanadate. Analysis of the data was performed as for the previous mutants combinations, with Figure 4A showing the amplitude average lifetime versus the acceptor molar ratio of the probe acceptor, with the deduced τ_{DA} values being reported in Table 3. Theoretical curves obtained when the molar ratio of the acceptor was plotted against the ratio of τ_{DA}/τ_D and compared with the experimental values obtained in the case of Cys-428−MIANS and Cys-428−DABMI (without any effector added) was then plotted in Figure 4B. Again, the results showed that the functional BmrA unit is a dimer. Similar results were found for the data obtained in the presence of each effector (not shown), indicating that their presence did not modify the oligomerization state of BmrA. As observed previously for the former mutant combinations, the distance between the two probes bound to Cys-428 of each BmrA monomer is compatible with the structure of BtuCD. Also, the presence of each effector did not seem to profoundly affect the proximity of the NBDs in the structure of the BmrA dimer (Table 3), yet

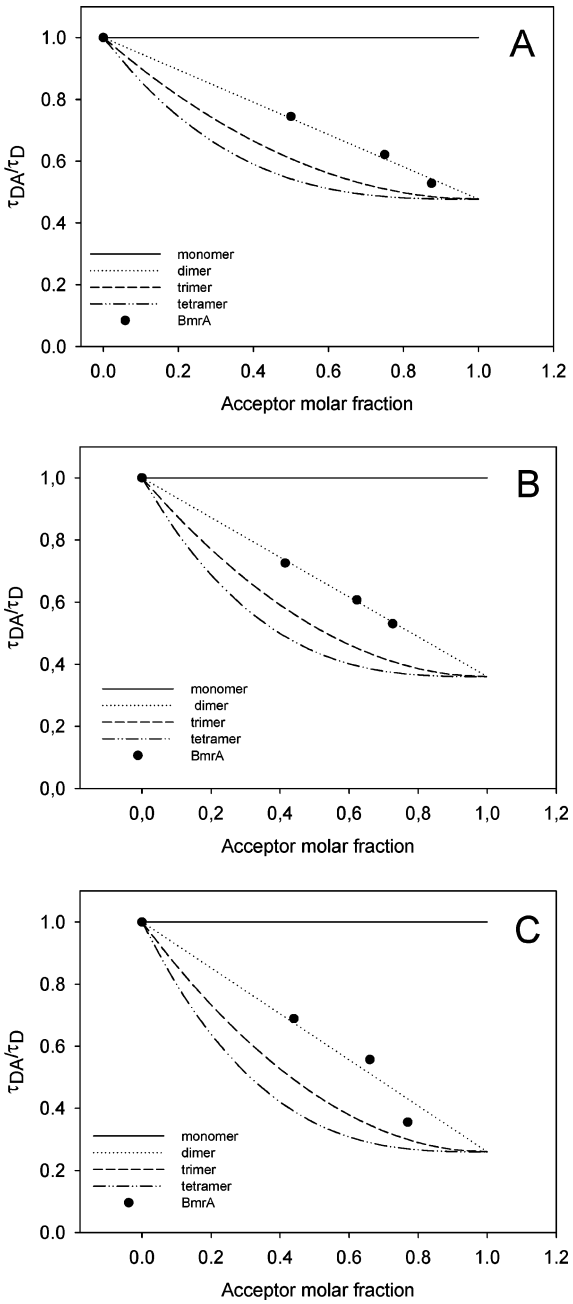

FIGURE 3: Transfer efficiency determination according to different models of BmrA oligomerization; evidence that BmrA is a homodimer. (A) τ_{DA}/τ_D of G473C−MIANS/G473C−DABMI is expressed as a function of the acceptor molar fraction; the theoretical curves were drawn as explained in the Experimental Procedures. B and C were the same as A but were obtained with T370C−MIANS/T370C−DABMI and G473C−MIANS/T370C−DABMI, respectively.

they significantly modify the FRET phenomenon, as revealed notably by the different $\langle\tau\rangle_a$ calculated for each effector. Thus, the bound chemical probes were sensitive to the conformational changes induced by the binding of each effector, although the overall structures of the BmrA dimers were essentially unchanged.

DISCUSSION

One of the main results that stems from this paper is that single labeling of BmrA monomer at three different sites, either Cys-370, Cys-473, or Cys-428, does not prevent its reassociation in a lipid bilayer environment and that the state of this association is dimeric, regardless of the probe combination used (Cys-370−MIANS + Cys-370−DABMI, Cys-370−MIANS + Cys-473−DABMI, or Cys-473−MIANS + Cys-473−DABMI). In the *E. coli* membrane, the overexpressed BmrA was previously shown to be fully functional and therefore adopted, at least, a dimeric organization (*22*, *23*). Consequently, this suggests that following DDM addition to solubilize the proteins, BmrA dimers are able to dissociate into monomers that, once labeled with the chemical probes, can reassociate upon detergent removal. Indeed, it was found that in the presence of 1% DDM, BmrA eluted from a gel-filtration FPLC column as a mixed population, with the main peak having an estimated molecular weight of ∼90 kDa and the minor peak eluting with an estimated molecular weight of ∼190 kDa (Dalmas et al., unpublished results). Clearly, the mass of the major peak is too small to correspond to a dimer (∼130 kDa) and most likely represents BmrA monomers associated with detergent molecules. Thus, this strongly argues that, in the presence of 1% DDM, BmrA exists as an equilibrium between monomers and dimers. Interestingly, the ATPase activity of the DDM-solubilized BmrA was only partially sensitive to vanadate inhibition (∼50% inhibition). Such a relative insensitivity to vanadate inhibition might be related to the vanadate insensitivity of the ATPase activity of isolated NBDs from several bacterial ABC transporters, which, in contrast to full-length transporters, do not hydrolyze ATP according to a mechanism of positive cooperativity (*35*−*37*). Reconstituted BmrA in proteoliposomes was also shown to hydrolyze ATP according to a mechanism of positive cooperativity and to be fully inhibited by vanadate (*22*), and one might postulate that the vanadate-insensitive part of ATPase activity in DDM-solubilized BmrA is due to the monomeric, noncooperative form of BmrA.

Another possible interpretation of the results reported here is that, upon reconstitution in proteoliposomes, BmrA exists as a mixture of monomer and higher-ordered complexes, and consequences for FRET analysis have been reviewed (*38*). Importantly, theoretical analysis revealed that a dimer is the only case where the efficiency of energy transfer versus the molar fraction of the fluorescence acceptor is linear, regardless of an equilibrium between a monomer and higher-ordered state of the protein studied (*39*). Therefore, the existence of a putative equilibrium for BmrA does not challenge that its functional oligomeric state in the membrane is a dimer. Furthermore, given that the ATPase activity of BmrA is quite high after reconstitution in proteoliposomes and that it could be fully inhibited by vanadate (*22*), we believed that it is unlikely that, upon reconstitution in proteoliposomes, BmrA remains partially present as a monomer.

A low-resolution 3D structure of BmrA previously obtained by cryoelectron microscopy had suggested a possible arrangement with a higher supramolecular organization, possibly a tetramer (*24*). Clearly, this possibility is not occurring here, and this tetrameric organization might have arisen from the molecular crowding because of the high ratio of protein over the lipid concentration used in the samples for electron microscopy. A dimeric state was also found for one of the BmrA closest homologues, LmrA, by measuring the rate of transport as a function of the ratio between the

Table 1: Steady-State Fluorescence Parameters and R_0 Calculations for Different BmrA Mutants Labeled with Either MIANS or DABMI (see the Experimental Procedures)[a]

	effector	quantum yield	spectral overlap integral, J (M^{-1} cm^{-1} nm^4)	R_0 (Å)
T370C-MIANS/T370C-DABMI		0.099	7.22746×10^{14}	31.0
T370C-MIANS/G473C-DABMI		0.099	7.04856×10^{14}	30.9
G473C-MIANS/G473C-DABMI		0.110	6.94506×10^{14}	31.4
S428C-MIANS/S428C-DABMI		0.082	8.5045×10^{14}	30.9
	ATP-Vi	0.076	8.75019×10^{14}	30.7
	ADP	0.079	8.63929×10^{14}	30.8
	40 μM doxorubicin	0.049	8.47203×10^{14}	28.4

[a] The values were obtained from the graphs shown in Figure 2A for the labeling of T370C by either MIANS or DABMI and from similar experiments for the other probe combinations and/or mutants.

Table 2: Sum of the Exponential Decay Analysis of the Fluorescence of Different BrmA Mutants Labeled with the Fluorescence Donor (MIANS) and Reconstituted into Proteoliposomes with Increasing Concentrations of BmrA Mutants Labeled with the Fluorescence Acceptor (DABMI)[a]

	acceptor molar fraction	lifetimes (ns)			pre-exponential factors				
		τ_1	τ_2	τ_3	α_1	α_2	α_3	$\langle\tau\rangle_a$	χ_r^2
G473C/G473C	0	9.371	4.352	1.051	0.1073	0.5136	0.2504	*4.022*	1.081
	0.5	8.389	3.683	0.9933	0.09434	0.4659	0.4145	*2.995*	0.993
	0.75	8.532	3.443	0.7872	0.06622	0.4874	0.5029	*2.498*	1.029
	0.875	9.762	3.424	0.8284	0.04152	0.4436	0.6893	*2.125*	0.972
T370C/T370C	0	10.98	4.636	0.7416	0.0798	0.5216	0.4163	*3.541*	0.941
	0.41	9.002	3.592	0.636	0.1151	0.4884	0.641	*2.57*	1.003
	0.62	12.7	3.891	0.5654	0.06687	0.4424	0.9319	*2.149*	1.018
	0.73	14.66	3.677	0.4323	0.06932	0.4553	1.181	*1.877*	0.861
T370C/G473C	0	10.90	4.56	1.246	0.0665	0.5553	0.2753	*4.013*	1.086
	0.44	9.865	3.722	0.8959	0.06233	0.5072	0.4972	*2.764*	0.928
	0.66	9.739	3.545	0.7691	0.05797	0.4861	0.6447	*2.342*	0.897
	0.77	7.812	2.702	0.3184	0.1042	0.5179	1.202	*1.423*	0.966
S428C/S428C	0	6.713	2.614		0.4453	0.3816		*4.821*	0.9303
	0.225	6.423	2.259		0.4383	0.4079		*4.415*	1.099
	0.45	5.011	1.946		0.3957	0.2593		*3.797*	0.984
	0.7875	3.865	0.9656		0.4177	0.2944		*2.666*	0.9655
S428C/S428C + ATP-Vi	0	6.869	2.961		0.267	0.4534		*4.409*	0.9917
	0.225	6.481	2.867		0.2714	0.4164		*4.268*	0.7823
	0.45	5.751	2.006		0.3311	0.3925		*3.719*	1.049
	0.7875	3.688	1.032		0.4203	0.3108		*2.559*	1.121
S428C/S428C + ADP	0	19.26	5.262	1.766	0.01226	0.4624	0.3843	*3.898*	1.125
	0.225	11.61	4.102	1.126	0.04136	0.5491	0.4023	*3.209*	1.022
	0.45	9.638	3.869	1.132	0.05602	0.4581	0.5021	*2.835*	0.994
	0.675	11.67	3.783	0.8487	0.03032	0.4795	0.6458	*2.35*	0.934
	0.7875	7.601	3.21	0.8613	0.09219	0.4124	0.8613	*1.854*	1.342
S428C/S428C + doxorubicin	0	9.205	3.808	0.5915	0.07663	0.4994	0.6706	*2.409*	0.921
	0.225	10.48	3.644	0.7328	0.03998	0.4863	0.6634	*2.25*	0.902
	0.45	8.208	3.128	0.7106	0.09147	0.4561	0.6786	*2.169*	1.062
	0.675	9.498	3.6	0.7596	0.04641	0.4292	0.7642	*2.07*	0.961

[a] The concentrations of ADP, ATP, Vi, and doxorubicin were 5 mM, 5 mM, 0.5 mM, and 40 μM, respectively.

wild-type and Cys mutant, with the latter being sensitive to inactivation by *N*-ethylmaleimide (*40*). Concerning ABC transporters as a whole, controversial results have been published in the literature regarding the quaternary structure of either full-length or half transporters. Hence, on the basis of radiation size inactivation, full-length *P*-glycoprotein has been postulated to exist *in vivo* as a dimer (*16*, *17*) and its oligomeric association has indeed been detected in a multidrug-resistant cell line (*15*). In contrast, a monomeric state has been proposed for the functional unit of *P*-glycoprotein based on either electron microscopy (*41*), lack of co-purification of *P*-glycoprotein with two different tags (*42*), or lack of co-immunopurification of differentially epitope-tagged *P*-glycoprotein molecules (*43*). Very recently, the oligomeric nature of a half-ABC transporter, ABCG2, was studied by different techniques after extraction from the membrane by using nondenaturing detergents, and it was concluded that this transporter exists mainly as a homotetramer (*21*). Although it is difficult to draw a definite conclusion about all of these studies, it is important to keep in mind that the use of membrane fractions highly enriched in one transporter might lead to nonphysiological association of the protein of interest, thereby resulting in artifactual interpretation of the supramolecular organization. Therefore, we favor the assumption that full-length or half-ABC transporters work *in vivo* as monomers or dimers, respectively.

A second conclusion that can be drawn from this study is that BmrA seems to preferentially adopt a closed conformation in the resting state (i.e., without added ATP-Mg), with its two NBDs close to each other. Such a conformation appears consistent with that found in BtuCD but in discrepancy with the closed conformation of *V. cholerae* MsbA. The latter has a quite unusual fold as compared to all other NBDs crystallized so far, with its Walker A and B motifs far apart in the structure of each monomer (*8*). The possibility

Table 3: Interresidue Distances Calculated from the FRET Experiments and a Comparison with the Three Available Structures of Full-Length ABC Transporters

BmrA dimer	substrate	R_0 (Å)	τ_{DA} (ns)	energy-transfer efficiency, E (%)	probe distance (Å)	interresidue distance[b] (Å)	equivalent distances in different 3D structures[a] (Å)		
							BtuCD	*V. cholerae* MsbA	*E. coli* MsbA
T370C−T370C		31.0	1.262	64.4	28	15−41	26	56.7	ND
G473C−G473C		30.9	1.921	74.3	31	18−44	29	38.9	118
T370C−G473C		31.4	1.031	52.3	25.9	13−39	39	60	ND
S428C−S428C		30.9	2.247	53.3	30	14−43	32.4	21	ND
	ATP-Vi	30.7	2.966	32.7	35	22−48			
	ADP	30.8	1.422	63.5	28	15−41			
	doxorubicin	28.4	1.883	21.8	35	22−48			

[a] Three-dimensional structures were downloaded from the Protein Data Bank using the accession numbers 1JSQ, 1PF4, and 1L7V for *E. coli* MsbA, *V. cholerae* MsbA, and BtuCD, respectively. The distances were obtained using WebLab Viewer (Molecular Simulations Inc.) software. ND, not determined because of the partially unresolved 3D structure of the NBD of *E. coli* MsbA. [b] Molecular dimensions of the fluorophores were calculated by molecular mechanics using ChemDraw (CambridgeSoft).

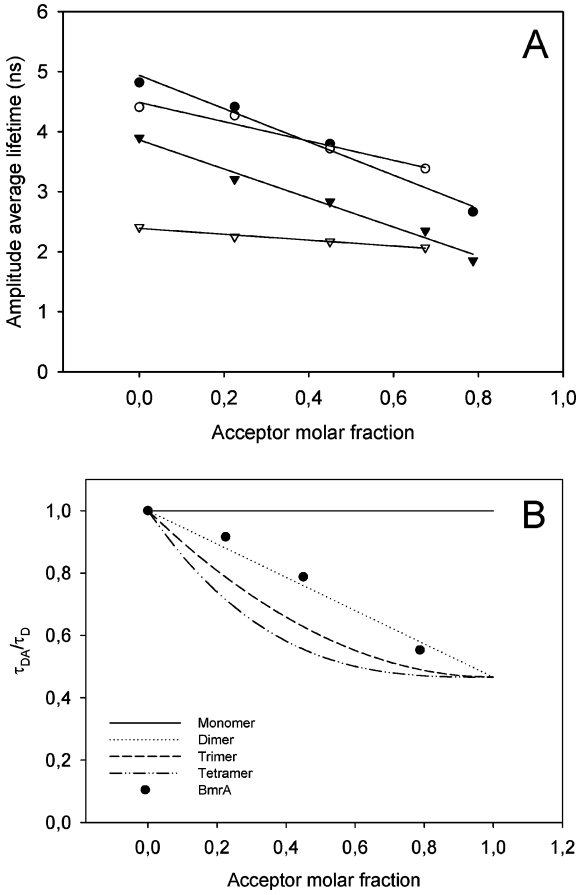

FIGURE 4: (A) Conformational changes induced by substrate binding to BmrA. Amplitude average lifetimes of S428C−MIANS versus S428C−DABMI molar fractions are shown. (●) Different lifetimes for the transporter in the absence of any exogenous substrate. Similar experiments were performed in the presence of ATP-Vi, ADP, and doxorubicin, and the amplitude average lifetimes for each condition were plotted as ○, ▼, and ▽, respectively. Prior to each measurement, proteoliposomes were incubated in the presence of DDM 0.01% (see The Experimental Procedures). (B) Evidence that S428C−MIANS/S428C−DABMI is a homodimer. τ_{DA}/τ_D of the labeled transporter is expressed as a function of the acceptor molar fraction, as described in Figure 3.

that BmrA switches between two closed conformations, one related to BtuCD and the other akin to *V. cholerae* MsbA, is also very unlikely. Indeed, if this was the case, one should expect that the distances extrapolated from the FRET measurements would comprise the values found for each of the closed 3D structures, weighted by the relative proportion of each conformation. However, the distances found here are very close to the one deduced from the BtuCD structure or even lower for the FRET experiment performed with the T370C and G473C mutants, ruling out the possibility that BmrA exists in equilibrium between these two conformations. Nevertheless, one cannot exclude that, in our preparation of BmrA reconstituted into liposomes, a minor proportion of BmrA dimers might exist in the open conformation related to that of *E. coli* MsbA. In this case, the two NBDs of BmrA would probably be much too far apart to give efficient FRET between the two bound probes (*32*). Related to this, we have been able to create an intramolecular disulfide bond between the first intracellular loop of the transmembrane domain and the NBD of BmrA based on the 3D structure of the open conformation of MsbA, indicating that BmrA can adopt a monomeric conformation related to that found in the open dimer of MsbA (O. Dalmas, A. Di Pietro, and J.-M. Jault, manuscript in preparation). Moreover, by using a site-directed spin-labeling approach, a recent report gave strong support to the occurrence of the open conformation of *E. coli* MsbA in a lipidic environment (*44*). As an alternative explanation, we cannot rule out the possibility that the tethering of the fluorescent probes to each BmrA mononer implies some constraints on the dimer, forcing it to adopt a more closed conformation than in the native, unmodified enzyme. However, in this case, the probability that the four different "constrained" conformations, using the four probe combinations, would all remain consistent with the closed structure of BtuCD is quite remote. Therefore, the results obtained here using FRET experiments are very likely relevant to the functional state of BmrA in the membrane.

ACKNOWLEDGMENT

We thank Dr. Qin Qu for helpful advice on FRET experiments, Gerry Prentice for the excellent LASER maintenance, and Dr. Alex Siemiarczuk (Photon Technology International, London, Ontario, Canada) for his kind advice on data processing.

REFERENCES

1. Higgins, C. F. (2001) ABC transporters: Physiology, structure, and mechanism−An overview, *Res. Microbiol. 152*, 205−210.

2. Linton, K. J., and Higgins, C. F. (1998) The *Escherichia coli* ATP-binding cassette (ABC) proteins, *Mol. Microbiol. 28*, 5−13.
3. Quentin, Y., Fichant, G., and Denizot, F. (1999) Inventory, assembly, and analysis of *Bacillus subtilis* ABC transport systems, *J. Mol. Biol. 287*, 467−484.
4. Borst, P., and Elferink, R. O. (2002) Mammalian ABC transporters in health and disease, *Annu. Rev. Biochem. 71*, 537−592.
5. Gros, P., Croop, J., and Housman, D. (1986) Mammalian multidrug resistance gene: Complete cDNA sequence indicates strong homology to bacterial transport proteins, *Cell 47*, 371−380.
6. Riordan, J. R., Rommens, J. M., Kerem, B., Alon, N., Rozmahel, R., Grzelczak, Z., Zielenski, J., Lok, S., Plavsic, N., Chou, J. L., et al. (1989) Identification of the cystic fibrosis gene: Cloning and characterization of complementary DNA, *Science 245*, 1066−1073.
7. Holland, I. B., and Blight, M. A. (1999) ABC-ATPases, adaptable energy generators fuelling transmembrane movement of a variety of molecules in organisms from bacteria to humans, *J. Mol. Biol. 293*, 381−399.
8. Davidson, A. L., and Chen, J. (2004) ATP-binding cassette transporters in bacteria, *Annu. Rev. Biochem. 73*, 241−268.
9. Jones, P. M., and George, A. M. (2004) The ABC transporter structure and mechanism: Perspectives on recent research, *Cell Mol. Life Sci. 61*, 682−699.
10. Smith, P. C., Karpowich, N., Millen, L., Moody, J. E., Rosen, J., Thomas, P. J., and Hunt, J. F. (2002) ATP binding to the motor domain from an ABC transporter drives formation of a nucleotide sandwich dimer, *Mol. Cell 10*, 139−149.
11. Chen, J., Lu, G., Lin, J., Davidson, A. L., and Quiocho, F. A. (2003) A tweezers-like motion of the ATP-binding cassette dimer in an ABC transport cycle, *Mol. Cell 12*, 651−661.
12. Chang, G., and Roth, C. B. (2001) Structure of MsbA from *E. coli*: A homolog of the multidrug resistance ATP binding cassette (ABC) transporters, *Science 293*, 1793−1800.
13. Locher, K. P., Lee, A. T., and Rees, D. C. (2002) The *E. coli* BtuCD structure: A framework for ABC transporter architecture and mechanism, *Science 296*, 1091−1098.
14. Chang, G. (2003) Structure of MsbA from *Vibrio cholera*: A multidrug resistance ABC transporter homolog in a closed conformation, *J. Mol. Biol. 330*, 419−430.
15. Poruchynsky, M. S., and Ling, V. (1994) Detection of oligomeric and monomeric forms of *P*-glycoprotein in multidrug resistant cells, *Biochemistry 33*, 4163−4174.
16. Boscoboinik, D., Debanne, M. T., Stafford, A. R., Jung, C. Y., Gupta, R. S., and Epand, R. M. (1990) Dimerization of the *P*-glycoprotein in membranes, *Biochim. Biophys. Acta 1027*, 225−228.
17. Jette, L., Potier, M., and Beliveau, R. (1997) *P*-glycoprotein is a dimer in the kidney and brain capillary membranes: Effect of cyclosporin A and SDZ-PSC 833, *Biochemistry 36*, 13929−13937.
18. Soszynski, M., Kaluzna, A., Rychlik, B., Sokal, A., and Bartosz, G. (1998) Radiation inactivation suggests that human multidrug resistance-associated protein 1 occurs as a dimer in the human erythrocyte membrane, *Arch. Biochem. Biophys. 354*, 311−316.
19. Rosenberg, M. F., Mao, Q., Holzenburg, A., Ford, R. C., Deeley, R. G., and Cole, S. P. (2001) The structure of the multidrug resistance protein 1 (MRP1/ABCC1). Crystallization and single-particle analysis, *J. Biol. Chem. 276*, 16076−16082.
20. Ferreira-Pereira, A., Marco, S., Decottignies, A., Nader, J., Goffeau, A., and Rigaud, J. L. (2003) Three-dimensional reconstruction of the *Saccharomyces cerevisiae* multidrug resistance protein Pdr5p, *J. Biol. Chem. 278*, 11995−11999.
21. Xu, J., Liu, Y., Yang, Y., Bates, S., and Zhang, J. T. (2004) Characterization of oligomeric human half-ABC transporter ATP-binding cassette G2, *J. Biol. Chem. 279*, 19781−19789.
22. Steinfels, E., Orelle, C., Fantino, J. R., Dalmas, O., Rigaud, J. L., Denizot, F., Di Pietro, A., and Jault, J. M. (2004) Characterization of YvcC (BmrA), a multidrug ABC transporter constitutively expressed in *Bacillus subtilis*, *Biochemistry 43*, 7491−7502.
23. Steinfels, E., Orelle, C., Dalmas, O., Penin, F., Miroux, B., Di Pietro, A., and Jault, J. M. (2002) Highly efficient over-production in *E. coli* of YvcC, a multidrug-like ATP-binding cassette transporter from *Bacillus subtilis*, *Biochim. Biophys. Acta 1565*, 1−5.
24. Chami, M., Steinfels, E., Orelle, C., Jault, J. M., Di Pietro, A., Rigaud, J. L., and Marco, S. (2002) Three-dimensional structure by cryo-electron microscopy of YvcC, an homodimeric ATP-binding cassette transporter from *Bacillus subtilis*, *J. Mol. Biol. 315*, 1075−1085.
25. Veatch, W., and Stryer, L. (1977) The dimeric nature of the gramicidin A transmembrane channel: Conductance and fluorescence energy transfer studies of hybrid channels, *J. Mol. Biol. 113*, 89−102.
26. Wu, P., and Brand, L. (1994) Resonance energy transfer: Methods and applications, *Anal. Biochem. 218*, 1−13.
27. Orelle, C., Dalmas, O., Gros, P., Di Pietro, A., and Jault, J. M. (2003) The conserved glutamate residue adjacent to the Walker-B motif is the catalytic base for ATP hydrolysis in the ATP-binding cassette transporter BmrA, *J. Biol. Chem. 278*, 47002−47008.
28. Chifflet, S., Torriglia, A., Chiesa, R., and Tolosa, S. (1988) A method for the determination of inorganic phosphate in the presence of labile organic phosphate and high concentrations of protein: application to lens ATPases, *Anal. Biochem. 168*, 1−4.
29. Urbatsch, I. L., Sankaran, B., Weber, J., and Senior, A. E. (1995) *P*-glycoprotein is stably inhibited by vanadate-induced trapping of nucleotide at a single catalytic site, *J. Biol. Chem. 270*, 19383−19390.
30. Kendall, D. A., and MacDonald, R. C. (1982) A fluorescence assay to monitor vesicle fusion and lysis, *J. Biol. Chem. 257*, 13892−13895.
31. James, D. R., Siemiarczuk, A., and Ware, W. R. (1992) Stroboscopic optical boxcar technique for the determination of fluorescence lifetimes, *Rev. Sci. Instrum. 63*, 1710−1716.
32. dos Remedios, C. G., and Moens, P. D. (1995) Fluorescence resonance energy transfer spectroscopy is a reliable "ruler" for measuring structural changes in proteins. Dispelling the problem of the unknown orientation factor, *J. Struct. Biol. 115*, 175−185.
33. Valeur, B. (2002) *Molecular Fluorescence: Principles and Applications*, Wiley-VCH, Weinheim, Germany.
34. Leveille-Webster, C. R., and Arias, I. M. (1995) The biology of the *P*-glycoproteins, *J. Membr. Biol. 143*, 89−102.
35. Morbach, S., Tebbe, S., and Schneider, E. (1993) The ATP-binding cassette (ABC) transporter for maltose/maltodextrins of *Salmonella typhimurium*. Characterization of the ATPase activity associated with the purified MalK subunit, *J. Biol. Chem. 268*, 18617−18621.
36. Nikaido, K., Liu, P. Q., and Ames, G. F. (1997) Purification and characterization of HisP, the ATP-binding subunit of a traffic ATPase (ABC transporter), the histidine permease of *Salmonella typhimurium*. Solubility, dimerization, and ATPase activity, *J. Biol. Chem. 272*, 27745−27752.
37. Sharma, S., and Davidson, A. L. (2000) Vanadate-induced trapping of nucleotides by purified maltose transport complex requires ATP hydrolysis, *J. Bacteriol. 182*, 6570−6576.
38. DeGrado, W. F., Gratkowski, H., and Lear, J. D. (2003) How do helix−helix interactions help determine the folds of membrane proteins? Perspectives from the study of homo-oligomeric helical bundles, *Protein Sci. 12*, 647−665.
39. Li, M., Reddy, L. G., Bennett, R., Silva, N. D., Jr., Jones, L. R., and Thomas, D. D. (1999) A fluorescence energy transfer method for analyzing protein oligomeric structure: Application to phospholamban, *Biophys. J. 76*, 2587−2599.
40. van Veen, H. W., Margolles, A., Muller, M., Higgins, C. F., and Konings, W. N. (2000) The homodimeric ATP-binding cassette transporter LmrA mediates multidrug transport by an alternating two-site (two-cylinder engine) mechanism, *EMBO J. 19*, 2503−2514.
41. Rosenberg, M. F., Callaghan, R., Ford, R. C., and Higgins, C. F. (1997) Structure of the multidrug resistance *P*-glycoprotein to 2.5 nm resolution determined by electron microscopy and image analysis, *J. Biol. Chem. 272*, 10685−10694.
42. Loo, T. W., and Clarke, D. M. (1996) The minimum functional unit of human *P*-glycoprotein appears to be a monomer, *J. Biol. Chem. 271*, 27488−27492.
43. Taylor, J. C., Horvath, A. R., Higgins, C. F., and Begley, G. S. (2001) The multidrug resistance *P*-glycoprotein. Oligomeric state and intramolecular interactions, *J. Biol. Chem. 276*, 36075−36078.
44. Buchaklian, A. H., Funk, A. L., and Klug, C. S. (2004) Resting state conformation of the MsbA homodimer as studied by site-directed spin labeling, *Biochemistry 43*, 8600−8606.
45. Thompson, J. D., Higgins, D. G., and Gibson, T. J. (1994) CLUSTAL W: Improving the sensitivity of progressive multiple sequence alignment through sequence weighting, position-specific gap penalties, and weight matrix choice, *Nucleic Acids Res. 22*, 4673−4680.

BI0482809